Martínez Marrero, Liset; Torres Gómez, Jorge; Dressler, Falko; Fernández-Getino García, M. Julia. (2022). Adaptive Blind MPSK Constellation Recovery and Equalization for Cognitive Radio Applications. *IEEE Transactions on Vehicular Technology, 71(11),* pp. 11988-12000.

Adaptive Blind MPSK Constellation Recovery and Equalization for Cognitive Radio Applications

L. M. Marrero, Jorge Torres Gómez, *Senior Member, IEEE*, Falko Dressler, *Fellow, IEEE*,
M. Julia Fernández-Getino García, *Member, IEEE*

Abstract—Cognitive radio (CR) is considered a relevant communication paradigm to deal with the increasing demands in modern communications systems. Adaptive schemes are required to recognize channel conditions and to properly adjust main transmission parameters to improve the quality of communications. In this direction, blind algorithms to recover constellation, from phase-modulated signals, represent a means to implement cognitive capabilities to allow automatic modulation recognition (AMR) on receivers. Commonly, the most popular approaches for blind constellation recovery are based on a two-step scheme. The first step uses to equalize channel effects and reduce inter-symbol interference (ISI). The second step carries out constellation recovery utilizing phase locked loop (PLL) systems like the Costas Loop, then to classify the incoming signal. This work proposes a novel single-step blind adaptive filter solution, inspired by an adaptive interference canceler, for joint equalization and constellation symbol recovery from received phase shift keying (PSK) waveforms. Furthermore, we propose new coefficients update mechanisms based on the constant amplitude of PSK signals. The proposed solution exhibits reduced computational complexity compared to the state of the art and a reduced time of convergence. Additionally, the proposed scheme does not require a training sequence to operate properly. The obtained results clearly show that the proposed scheme significantly improves accuracy regarding phase symbol estimation and ISI reduction.

Index Terms—LMS, adaptive filter, blind symbol phase estimation, PSK.

I. INTRODUCTION

THE huge increase in the number of wireless connected devices for daily use is facing the scarcity of limited spectrum resources [1]. By 2023, the total of connected machine to machine (M2M) and internet of things (IoT) devices is predicted to be 14.7 billions [2]. Dealing with the reduced availability of connections, cognitive radio (CR) offers mechanisms to support smart and dynamic policies

Liset Martínez Marrero is with Intelligent Sensors and Networks (CC-ISN), Lucerne University of Applied Sciences and Arts, HSLU, Switzerland e-mail: liset.martinezmarrero@hslu.ch

Jorge Torres Gómez is with the School of Electrical Engineering and Computer Science, TU Berlin, Berlin, Germany: torres-gomez@ccs-labs.org

Falko Dressler is with the School of Electrical Engineering and Computer Science, TU Berlin, Berlin, Germany: dressler@ccs-labs.org

M. Julia Fernández-Getino García is with the Department of Signal Theory and Communications, Carlos III University of Madrid 28911, Leganés, Madrid, Spain, mjulia@tsc.uc3m.es
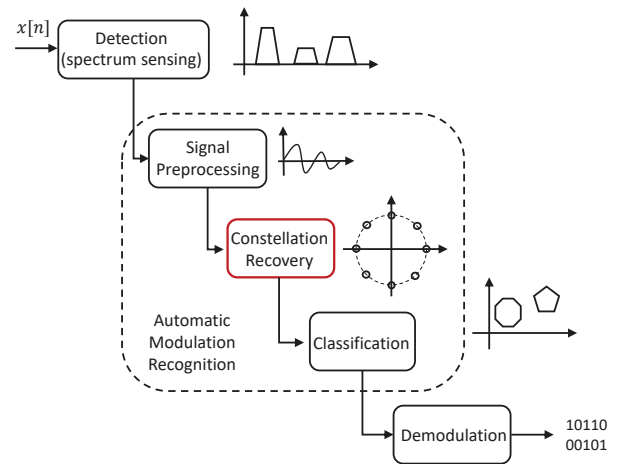
Fig. 1. Block diagram for the CR-receiver operation.

accounting for a flexible spectrum usage [3]. CR is supported by dynamical mechanisms allowing to re-adapt transmitters and receivers on the physical (PHY), medium access control (MAC), and network layers [4].

In the PHY layer, CR devices are conceived with autonomous capabilities to select communication parameters as the frequency band to operate, the modulation format, or the coding scheme. In this way, the receiver-side must be equipped with robust methods to detect and identify the received signal to dynamically adjust the received parameters [5]. To illustrate, Fig. 1 depicts the variety of components a CR receiver may perform partially or completely (i.e., as a full CR or "Mitola radio" [6]). Incoming signals are detected through spectrum sensing (SS) operations, then the received modulation is identified through automatic modulation recognition (AMR) methods, and finally, the carried information may be decoded autonomously [7]. These components may be used to autonomously decode the emitted information as an ultimate goal or to provide awareness about the channel status: spectrum occupancy [8], modulation format, information rate of emitted signals, etc [9].

Specifically, AMR mainly concerns two steps, namely, the signal preprocessing and the classification algorithm that can include feature extraction (illustrated in Fig. 1 as the constellation recovery block) [7]. Signal preprocessing copes with undesirable channel effects conceiving noise reduction and channel equalization techniques, as well as signal parameter estimation. Classification algorithms, comprised of likelihood and feature-based techniques, estimate the transmitted modu-

lation format thereafter.

This paper focuses on AMR techniques concerning feature extraction for the signal classification step. Specifically, we address techniques to recover constellation points from phase shift keying (PSK) waveforms and illustrate its applicability to quadrature amplitude modulation (QAM) as well. Based on the recovered constellation, a variety of classification techniques (cf. [7]) can be applied to distinguish the received signal from binary phase shift keying (BPSK), quadrature phase shift keying (QPSK), 8PSK, or QAM. Moreover, the recovered constellation points can be used as a signal feature to distinguish primary users (PUs) from secondary users (SUs). That is, the use of a given frequency band by PUs can be better identified not only by its occupancy, but also through the modulation format used by the PU. Furthermore, the recovered constellation points can be used to determine the mobile or static condition of the PU based on the rotation of the received constellation points as an additional feature [10].

In the literature, reported methods to recover phase from PSK or QAM waveforms are mainly conceived through phase locked loop (PLL) like the Costas Loop [11]. These are also conceived with the inclusion of signal preprocessing methods like channel equalizers and filters to reduce the impact of noise and undesirable channel effects [7]. However, these techniques introduce processing delays and further inter-symbol interference (ISI) produced by the phase response and the limited bandwidth of the used linear time invariant (LTI) filters, respectively [12]. The induced delay incurs in a limited convergence time, while ISI incurs in a degraded performance to later classify the received signal.

In a different approach, we introduce a method based on adaptive filter (AF) techniques, avoiding the use of LTI-filters and thereby shortening the processing delay. AF have been widely employed on several signal processing applications such as equalization [13] and tracking of signal parameters [14]. Still, its inherent adaptation process makes AFs also a potential candidate for phase recovery applications.

We report a new solution based on the adaptive noise canceler model by Widrow *et al.* [15]. The proposed AF-based scheme can be implemented with a classical update mechanism, such as least mean squares (LMS), but we also introduce novel coefficients update mechanisms that report considerable benefits to accelerate the rate of convergence. This newly proposed solution is based on an adaptive noise canceler filter where processing is carried out with constant modulus coefficients and it is then denoted as CMC. Furthermore, taking advantage of the constant amplitude of PSK waveforms, the use of the CMC method implicitly introduces a channel equalization mechanism to some extent. That is, a preprocessing technique is jointly applied when using these adaptive techniques to adjust the filter coefficients. We confirm the feasibility and performance of our proposed techniques using analytic and geometrical descriptions, as well as simulation results.

Our main contributions can be summarized as follows:
- we introduce a low complex AF technique for the constellation recovery of PSK signals;
- we extend this method to recover the constellation points

of QAM waveforms;
- we present a new update mechanism, namely CMC, to increase the convergence speed of the filter in comparison to the traditional LMS technique;
- we show how CMC also introduces a channel equalization mechanism to some extent; and
- we compare the impact of realistic channel models to recover the constellation points.

The remainder of the paper is structured as follows. First, related work is discussed in Section II. Then, the system model is presented in Section III to analytically describe waveforms and the implemented AF structure. The AF's coefficients are updated following the proposed CMC mechanisms in Section IV with an illustrative example to discuss its functioning and performance in Section V. Then, the resulting performance is shown through learning curves, constellation points, and eye-patterns using realistic channel models in Section VI. Finally, Section VII concludes the paper and summarizes some future directions.

II. RELATED WORK

Reported solutions to recover constellation points for PSK and QAM waveforms are mainly based on PLL schemes, such as a Costas Loop [16] and a Square Loop [17], or through the maximum likelihood (ML) [18] method. All of which are using an equalization for undesirable channel effects in the signal preprocessing step (cf. Fig. 1). The use of PLL and Costas Loop schemes are one of the most employed methods to track the phase of incoming signals without training sequences [11]. Although ML affords the best performance, its implementation is typically prohibitive due to the total number of multiplications, exponent arithmetic operations, and integration procedures.

As depicted in Fig. 2 a), the Costas Loop decomposes the received waveform for in-phase and quadrature components, from which the received constellations points can be decoded. The feedback loop through the error detector, loop filter, and numerically controlled oscillator (NCO) replicates the carrier frequency of the emitted waveform. The in-phase and quadrature branches recover the constellation points after a down-conversion operation through the multipliers and filters blocks.

Using a single loop PLL, the constellation points of the received signal can also be estimated [12], but its applicability is usually limited to BPSK waveforms. As depicted in Fig. 2 b), the input BPSK signal is squared to remove the carried data (binary) then allowing the PLL to track only the instantaneous phase of the carrier (at twice the original carrier frequency). The PLL output signal is then used to recover the constellation points after a frequency division by two.

These two schemes exhibit two major drawbacks. Although they are less complex than the ML detector, they still require down converters, which in turn incur in filter blocks implementation (second-order at least) with the corresponding implementation of adders and multipliers. Besides, the use of filters inherently introduces ISI and delay in the processing chain [12]. As long as filtering reduces the bandwidth of
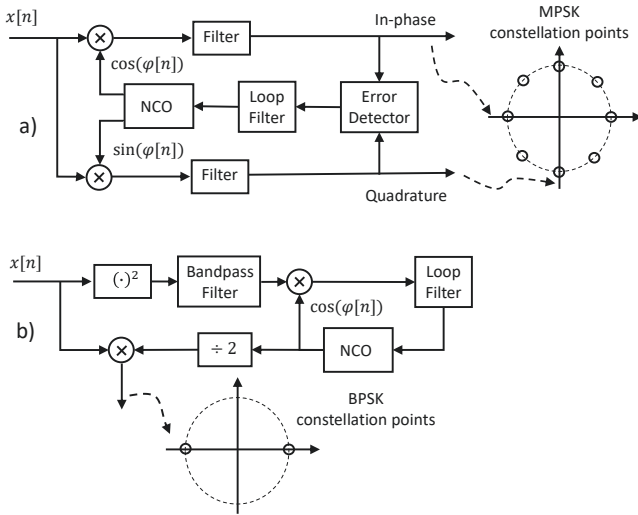
Fig. 2. Block diagrams to recover PSK constellation points, where $\varphi[n]$ represents the phase at the output of the NCO. a) Costas Loop. b) Square Loop.

the recovered message, it becomes a symbol-spreader, and inevitably it will also introduce delay due to the non-zero group delay response.

Furthermore, in front of the constellation recovery, equalization methods are typically included to compensate for dispersive channels and reduce ISI. The preferred solutions to blindly compensate channel effects rely on adaptive filtering to equalize the amplitude of incoming phase-modulated signals. The most popular ones are based on Godard's constant modulus algorithm (CMA), Shalvi-Weistein (SWA), and minimum entropy criterion (MED) [19] algorithms. These solutions are based on the constant amplitude of phase-modulated signals such as PSK waveforms. These algorithms establish cost functions to adjust the norm of received signals to a constant value, then to correct induced amplitude variations of multipath channels. Other CMA-based algorithms have been also defined to improve the convergence rate and performance. Those are the least squares (LSCMA), QR decomposition (QR-CMA), recursive (RCMA), recursive least squares (RLSCMA), and orthogonalized (O-CMA) [20].

III. SYSTEM MODEL

Considering PSK signals, the discrete waveform representation is expressed by $x[n] = A\cos(w_c n + \varphi[n])$, where A is the signal amplitude, w_c is the carrier frequency and $\varphi[n]$ denotes the time-varying symbol phase values in a finite set of M phases. This waveform carries information on the symbol phase parameter $\varphi[n]$.

In the case of PSK signals, symbols can be described by the *in phase* $I[n]$ and *quadrature* $Q[n]$ components as [21]

$$x[n] = I[n]\cos(\omega_c n) - Q[n]\sin(\omega_c n), \qquad (1)$$

where

$$\begin{aligned} I[n] &= A\cos(\varphi[n]), \qquad (2) \\ Q[n] &= A\sin(\varphi[n]). \end{aligned}$$
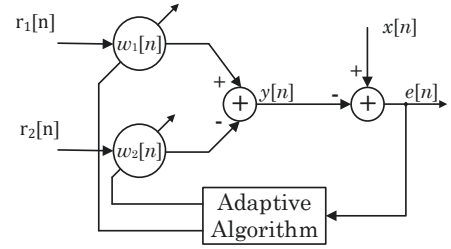

Fig. 3. Notch adaptive filter scheme [15].

In the case of the AF (notch filter scheme), it is conceived by two reference signals, $r_1[n]$ and $r_2[n]$, and two filter coefficients, $w_1[n]$ and $w_2[n]$, as depicted in Fig. 3 [15]. Given a single-frequency interference tone in $x[n]$, the filter output conforms a similar sequence $y[n]$ based on the adjusted coefficients and the reference signals. That is, the resulting output sequence $y[n]$ will estimate the incoming signal $x[n]$ as long as the adaptive algorithm operates to reduce the power of the error sequence $e[n]$ [14].

Besides, provided that the output filter computes

$$y[n] = w_1[n]\,r_1[n] - w_2[n]\,r_2[n], \qquad (3)$$

the filter coefficients $w_1[n]$ and $w_2[n]$ might estimate the in phase and quadrature components according to a direct comparison between Eq. (1) for the received PSK signal and Eq. (3) for the AF output as

$$x[n] = \underbrace{I[n]}_{w_1[n]}\overbrace{\cos[\omega_c n]}^{r_1[n]} - \underbrace{Q[n]}_{w_2[n]}\overbrace{(\sin[\omega_c n])}^{r_2[n]}, \qquad (4)$$

where the coefficients $w_1[n]$ and $w_2[n]$ are used to estimate $I[n]$ and $Q[n]$ from the received signal whenever the reference signals $r_1[n]$ and $r_2[n]$ are equal to $\cos[\omega_c n]$ and $\sin[\omega_c n]$, respectively. Then, based on the scheme in Fig. 3, we propose to directly recover the constellation points from received PSK signals as $(I[n], Q[n])$ through the coefficient pair $(w_1[n], w_2[n])$.

Through the adaptive filter scheme in Fig. 3 little knowledge is required about the received PSK signal. Without resorting to training sequences, this system allows in-phase and quadrature carrier components to recover. Through this scheme, the signal parameter to be given at the receiver side is the carrier frequency ω_c for the reference signals $r_1[n]$ and $r_2[n]$.

The AF scheme in Fig. 3 represents a Notch configuration similar to the system presented in [15]. This scheme is typically used to cancel interference tones on a variety of applications. Recent works show significant results estimating the carrier frequency of a single complex sinusoid with a Notch filter and the recursive least squares (RLS) algorithm [22]. To the best of our knowledge, none of the consulted works has focused on recovering the phase of a given sinusoidal signal to estimate the constellation points of PSK waveforms.

IV. COEFFICIENTS UPDATE MECHANISM: CMC

Reported solutions based on the AF scheme in Fig. 3 commonly implement LMS and RLS algorithms to update

the weighting coefficients pair $(\omega_1[n], \omega_2[n])$ [22]. However, a new updating mechanism may be devised by including additional constraints to improve the convergence rate.

When the received signal $x[n]$ represents a PSK waveform, the AF coefficients will be located over a circumference of radius A due to the constant amplitude of these waveforms. In this respect, a new restriction is included when limiting the location of the coefficients to be on a circumference (i.e., coefficients of constant modulus). Similar to the CMA acronym (constant modulus algorithm), this new solution is referred to as constant modulus coefficients (CMC).

A. The CMC Concept

Considering the AF structure in Fig. 3, its two coefficients' trajectory can be restricted to a circumference of constant radius, as given by the amplitude of the received PSK waveform. To illustrate this mechanism, Fig. 4 provides a geometrical representation in the case of BPSK signals, where the points S_1 and S_2 represent the steady state constellation points. Following this reasoning, the point c must be guided, over the circumference of radius A (amplitude of PSK waveform), to either points S_1 or S_2 whenever the incoming phase is 0 or π, respectively. Similar to the LMS algorithm, the direction of movement of the point c is provided by the opposite direction of a given gradient vector $-\widehat{\nabla}\mathbf{J}[n]$, which indicates the direction of the minimum value of the error signal $e[n]$ (cf. Fig. 3). Considering the two coefficients filter in Fig. 3, this gradient vector is defined by two components $\widehat{\nabla}\mathbf{J}[n] = [\widehat{\nabla}J_1[n] \ \widehat{\nabla}J_2[n]]$.

Based on this geometrical representation, a new intuitive mechanism to update the phase of point c is based on the projection of $-\widehat{\nabla}\mathbf{J}[n]$ over a vector $\mathbf{T}$, which is tangent to the circumference as represented in Fig. 4 for the transition between S_1 and S_2. The projection $-\widehat{\nabla}\mathbf{J}_T[n] = \left\langle -\widehat{\nabla}\mathbf{J}[n], \mathbf{T} \right\rangle$, indicates the counterclockwise rotation of c indicating the next step coordinates for the point c. The Fig. 4 depicts the case where $-\widehat{\nabla}\mathbf{J}[n]$ has a positive projection on the tangent vector $\mathbf{T}$. This is the case where a symbol of negative phase, from a given BPSK signal, is after a symbol of positive phase. Under these conditions, the phase of the point c is updated to the counterclockwise direction over the circumference of radius A. These geometrical mechanisms represent the fundamentals of the proposed solution to update the two AF coefficients. At this point, we remark the need to estimate the amplitude of the received PSK waveform, which can be directly derived following the CMA algorithm as $\frac{\mathbb{E}\{x^4[n]\}}{\mathbb{E}\{x^2[n]\}}$ [23].

Following the geometrical representation in Fig. 4, to derive the equations to update the AF coefficients, we depart from the relation

$$w_1[n] = A\cos(\widehat{\varphi}[n]), \qquad (5)$$
$$w_2[n] = A\sin(\widehat{\varphi}[n]),$$

where $\widehat{\varphi}[n]$ is the parameter to be updated in order to find a closer similarity to the original transmitted phase sequence $\varphi[n]$. Based on these parametric relations, a rule must be established to update $\widehat{\varphi}[n]$ for each adaptive iteration when decrementing the amplitude of the error sequence $e[n]$. To do
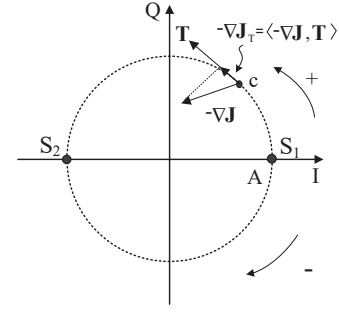

Fig. 4. Illustration of the proposed CMC updating mechanism.

so, we use the sign of the projected gradient vector $(-\widehat{\nabla}\mathbf{J}_T[n])$ to indicate the counter or the clockwise direction of $\widehat{\varphi}[n]$, and the magnitude of the gradient vector $(\parallel \widehat{\nabla}\mathbf{J}[n] \parallel)$ to quantify the step to afford in the next iteration as

$$\Delta\widehat{\varphi}[n] = \mu\,\mathrm{sign}\left(-\widehat{\nabla}\mathbf{J}_T[n]\right)\frac{\parallel \widehat{\nabla}\mathbf{J}[n] \parallel}{J_{max}}\pi, \qquad (6)$$

where μ is the step size, $\parallel \widehat{\nabla}\mathbf{J}[n] \parallel$ is the magnitude of gradient vector $\widehat{\nabla}\mathbf{J}[n]$, $\mathrm{sign}\left(-\widehat{\nabla}\mathbf{J}_T[n]\right)$ establishes the proper counterclockwise or clockwise direction, where $\mathrm{sign}(\cdot)$ denotes the sign operation, J_{max} represents the maximum value of $\parallel \widehat{\nabla}\mathbf{J}[n] \parallel$, and $\frac{\parallel\widehat{\nabla}\mathbf{J}[n]\parallel}{J_{max}}$ indicates the angle as a fraction of π to be updated.

According to this coefficient update mechanism, the product of both terms $\mathrm{sign}\left(-\widehat{\nabla}\mathbf{J}_T[n]\right)$ and $\frac{\parallel\widehat{\nabla}\mathbf{J}[n]\parallel}{J_{max}}$ provides a normalized quantity on the interval $[-1, 1]$. Having this as a resultant factor of π, as indicates Eq. (6), it is interpreted as the phase in the interval $[-\pi, \pi]$, and accordingly as a movement over the circumference in Fig. 4.

The gradient vector $\widehat{\nabla}\mathbf{J}[n]$ is computed similarly to the LMS algorithm as

$$\widehat{\nabla}J_{1,2}[n] = \frac{\mathrm{d}\,e^2[n]}{\mathrm{d}w_{1,2}} = 2e[n]r_{1,2}[n], \qquad (7)$$

where $r_1[n] = \cos(wn)$ and $r_2[n] = \sin(wn)$ are defined in accordance to (4) and $e[n] = x[n] - y[n]$ as represented in the scheme depicted in Fig. 3. Finally, the proposed updating mechanism is derived from (6) yielding to the new updating mechanism as

CMC-1

$$\widehat{\varphi}(n+1) = \widehat{\varphi}(n) - \mu\,\mathrm{sign}\left(-\widehat{\nabla}\mathbf{J}_T[n]\right)\frac{\parallel \widehat{\nabla}\mathbf{J}[n] \parallel}{J_{max}}\pi, \quad (8)$$

However, after evaluating this mechanism in simulations (not illustrated here), results indicates that Eq. (8) produces abrupt changes on the filter output $y[n]$ due to large values of $\parallel \widehat{\nabla}\mathbf{J}[n] \parallel$. These abrupt changes on $y[n]$ cause distortion on recovered symbols. To avoid this inconvenient result, we may reduce the abrupt changes produced by $\parallel \widehat{\nabla}\mathbf{J}[n] \parallel$ with two other updating mechanisms. As a first approach, the norm is replaced by the minimum value of the components yielding

CMC-2

$$\widehat{\varphi}(n+1) = \widehat{\varphi}(n) - \tag{9}$$
$$- \mu \operatorname{sign}\left(-\widehat{\nabla}\mathbf{J}_T[n]\right) \frac{\min(J_1[n], J_2[n])}{J_{max}} \pi.$$

As a second approach, the norm is replaced by the average value of its components as

CMC-3

$$\widehat{\varphi}(n+1) = \widehat{\varphi}(n) - \tag{10}$$
$$- \mu \operatorname{sign}\left(-\widehat{\nabla}\mathbf{J}_T[n]\right) \frac{(J_1[n] + J_2[n])/2}{J_{max}} \pi.$$

where $\| \widehat{\nabla}\mathbf{J}[n] \|$ has been replaced by new terms as $\min(J_1[n], J_2[n])$ and $(J_1[n]+J_2[n])/2$ for CMC-2 and CMC-3, respectively. Both equations in (9) and (10) reduce the total updated amount $\Delta\varphi[n]$ in comparison to (8). It is straightforward to establish that the minimum and average value of components of $\widehat{\nabla}\mathbf{J}[n]$ is always smaller than the norm of the same vector $\| \widehat{\nabla}\mathbf{J}[n] \|$.

These new two terms have the same role of the gradient vector $\widehat{\nabla}\mathbf{J}[n]$ to reduce the error sequence. The larger the value of $\| \widehat{\nabla}\mathbf{J}[n] \|$ is, the larger the values of $\min(J_1[n], J_2[n])$ and $(J_1[n]+J_2[n])/2$ will be, i.e., larger error values will produce larger update steps $\Delta\varphi[n]$, likewise lower errors will reduce $\Delta\varphi[n]$ accordingly.

On the other hand, the step-size μ is in the interval $0 < \mu < \frac{1}{\lambda_{max}}$, where λ_{max} is the largest eigenvalue of the autocorrelation matrix corresponding to the incoming signal $x[n]$ (similar to the LMS method). Given that the received waveform is conformed by a single frequency tone ω_c, then the autocorrelation matrix, in case of a two coefficients filter, is given as [24]

$$\mathbf{R}_{xx} = \begin{bmatrix} \frac{A^2}{2} & \frac{A^2}{2}\cos(2\omega_c) \\ \frac{A^2}{2}\cos(2\omega_c) & \frac{A^2}{2} \end{bmatrix}, \tag{11}$$

where the largest eigenvalue is computed by solving the characteristic equation $|\mathbf{R}_{xx} - \lambda\mathbf{I}| = 0$ yielding

$$\lambda_{max} = (1 + |\cos(2\omega_c)|), \tag{12}$$

where $\mathbf{I}$ represents the identity matrix.

B. Remarks

The new adaptation mechanisms CMC-1 to CMC-3 take advantage of the constant amplitude of PSK signals. This constant amplitude of the updating mechanism implicitly establishes that the recovered constellation points lie on a circumference of radius A, where A is the PSK signal amplitude. In comparison to the traditional LMS algorithm, the newly proposed mechanisms have to adjust only phase but not amplitude. This increases information and then reduces variance on estimating the transmitted components [25], which in turn will be in favor of the convergence speed.

Additionally, establishing a constant amplitude for the adaptive coefficients reduces the impact of distortions in the communication channel. Provided that the non-desirable effect of channels modifies the amplitude of received signals, i.e., multipath trajectory, the proposed scheme estimates a signal $y[n]$ of constant amplitude instead. In this concern, the proposed solution exhibits to have some countermeasure mechanism against, as later illustrated for a variety of channel models in Section VI.

C. Complexity Analysis

The proposed system in Fig. 3 is conceived with a finite impulse response (FIR) filter of two coefficients and the adaptive algorithm block. The adaptive algorithm may be implemented by using the proposed CMC methods or the traditional LMS mechanism. Complexity regarding CMC methods is superior to the equivalent LMS algorithm given that the proposed adaptive algorithm performs more operations than the LMS method. By comparing expressions from the CMC methods in (8), (9), and (10) with the standard LMS given by $\widehat{\mathbf{w}}[n+1] = \widehat{\mathbf{w}}[n] + \mu\mathbf{r}[n]e[n]$ [15], the superior performance of CMC is attained at the expense of a few additional terms to update the coefficients. Bold letters $\mathbf{w}$ and $\mathbf{r}$ represent vectors of components $\mathbf{w} = [w_1[n], w_2[n]]$ and $\mathbf{r} = [r_1[n], r_2[n]]$.

Regarding the previously reported schemes, common systems for constellation points recovery implement two main subsystems comprising channel equalization, to counteract undesirable channel effects, and phase recovery methods like the Costas Loop scheme. For instance, to compensate channel effects, CMA techniques implement a FIR filter of complex taps in addition to the adaptive coefficients mechanism. This to reduce undesirable channel effects [26]. In addition, the Costas Loop scheme is used to recover the constellation points, which in turn implements two-phase detectors and NCO blocks, as depicted in Fig. 2. The phase detector is commonly implemented by a multiplier and a low pass filter of at least second-order. In this regard, the use of these subsystems has larger complexity than the proposed scheme in Fig. 3 by either using LMS or CMC methods.

D. Extension to QAM Constellation Recovery

The proposed AF-based scheme and the coefficients update mechanisms can be also extended to estimate the constellation points from QAM waveforms. Since its constellation points are located over circumferences with different radius, as represented in Fig. 5, then a parallel operation of AF can be used to derive the constellation points per circumference. As depicted in this figure, each adaptive filter will operate with reference signals $(r_1[n], r_2[n])$ according to each different radius on the constellation points, in this case A_1, A_2, A_3. Then by comparing the energy of each different error signal $e[n]$, the radius can be selected according to that one with the less error amplitude (Radius detector block). The multiplexer (MUX block) will output the coefficient pair $(\omega_1[n], \omega_2[n])$ in accordance with the received symbol.

Although directly extensible to QAM waveforms, the complexity and performance of the scheme in Fig. 5 in comparison to the traditional Costas Loop should be further analyzed in a separate work. However, at this point, it can be remarked
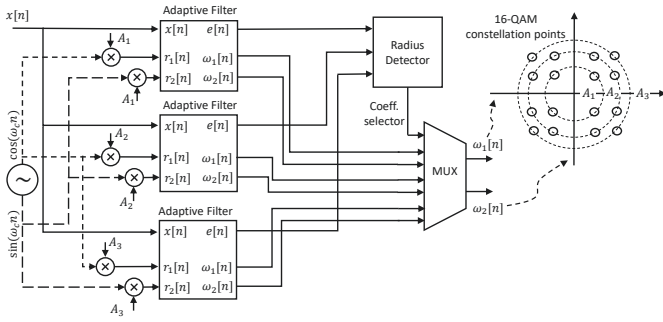
Fig. 5. Block diagram for 16-QAM constellation recovery.

the inherent reduction of channel distortions as long as the provided constellation points are fixed to each different circumference when implementing the conceived CMC methods.

V. ILLUSTRATIVE EXAMPLE FOR QPSK AND QAM WAVEFORMS

Here we illustrate the functioning of the proposed scheme in Fig. 3 and the updating mechanism CMC-1 according to Eq. (8). It is assumed that a PU is transmitting either QPSK or QAM waveforms, where the carrier frequency is $\omega_c = \frac{\pi}{8}$. We assume that both waveforms are already represented in the discrete domain, i.e., the received signal has been already sampled by a previous analog to digital converter (ADC) block fulfilling the Nyquist criterion constraint. According to the relation $\omega_c = 2\pi \frac{f_c}{f_s} = \frac{\pi}{8}$ may correspond to baseband signals with a carrier frequency of $f_c = 1.25$ MHz and sampling frequency $f_s = 20$ MHz. This sampling frequency is according to typical bandwidths of CR networks, i.e. 4 MHz when the CR system is operating with global system for mobile communications (GSM) systems [27], or in the range 6–8 MHz for the IEEE 802.22 standard using the white space of television emissions [28]. There are also commercial available ADCs of 20 Msps and 12–16 bits resolution [29].

A. QPSK constellation recovery

We consider a QPSK signal with amplitude $A = 1$ and carrying the phase sequence $\varphi[n] = \{0, \frac{\pi}{2}, \pi, \frac{3\pi}{2}\}$. The QPSK waveform and the corresponding in phase and quadrature components are illustrated in Fig. 6, where Fig. 6 a) shows the transmitted QPSK waveform, while Fig. 6 b) and c) show the transmitted in phase and quadrature components. Each figure depicts the corresponding recovered signals with dashed lines, considering the proposed AF-based scheme. Here we illustrate results with rectangular pulses to better depict the convergence of the AF-based scheme. Although in realistic communication systems pulse shape mechanisms are used to reduce the impact of ISI, e.g. raised cosine pulses [30], the use of rectangular pulses lets to illustrate better the convergence behavior of the proposed scheme. Otherwise the convergence-rate performance will be masked by the pulse shape.

The recovered phase and quadrature components in Fig. 6 b) and c), are given by the two filter coefficients $w_1[n]$ and $w_2[n]$ from the proposed AF-based scheme shown in Fig. 3. Both filter coefficients track the in-phase and quadrature components of the transmitted signal to reduce the MSE
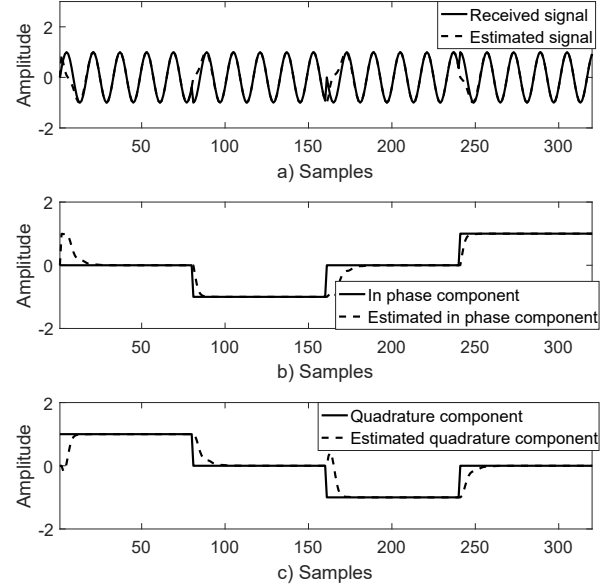

Fig. 6. Illustrative example to recover in phase and quadrature components of a QPSK waveform. a) Transmitted and recovered QPSK signal. b) Transmitted and recovered in phase component. c) Transmitted and recovered quadrature component.

between the transmitted signal $x[n]$ in (1) and the output filter $y[n]$ in Eq. (3).

The dynamics of the two coefficients on the constellation diagram are illustrated in Fig. 7 for CMC-1. In this case, seven iterations have been plotted based on the first seven samples of the received QPSK signal in Fig. 6 a). Provided the phase of the corresponding symbol is $\frac{\pi}{2}$, then the estimated constellation points are displaced from the starting point $(1, 0)$ to $(0, 1)$ on each iteration. The red points below the x-axis correspond to the second and third iterations, they were erroneously located due to the stochastic gradient noise [15]. Except for these two points, the rest have a positive projection of $-\widehat{\nabla}\mathbf{J}[n]$ (black vectors) over the tangent vector $\mathbf{T}$ (blue vectors), which in turn produces a counterclockwise movement as exhibit the next iterations following the red points.

On the other hand, Fig. 8 shows the dynamics of AF coefficients considering LMS and CMC methods when the arrived constellation point is $(0, -1)$ and the signal to noise ratio (SNR) is 10 dB for the first 15 iterations. Starting at point $(1, 0)$, the four algorithms seek the point $(0, -1)$ on each iteration. However, most of the time the CMC trajectories according to (8), (9), and (10) stay closer to the desired value $(0, -1)$ than the LMS method. This partial result shows that the proposed solution has a higher convergence rate than LMS.

The proximity of CMC and LMS output to desired values is better illustrated in Fig. 9, where the recovered signals are presented. Fig. 9 a) shows the output signal of the adaptive filter, from the scheme in Fig. 3, and the transmitted single frequency tone. All CMC methods get closer to the desired signal in a shorter period compared to the LMS method. Fig. 9 b) depicts the error signal of the AF-based schemes, where differences between the transmitted signal and the filter
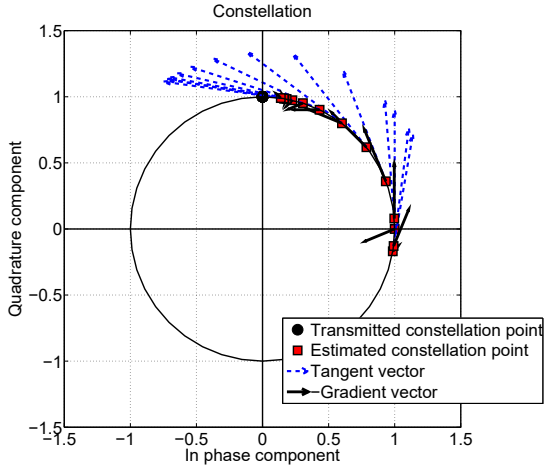
Fig. 7. Dynamics in the I-Q plane of the proposed AF-based solution considering CMC and LMS mechanisms for a QPSK signal.
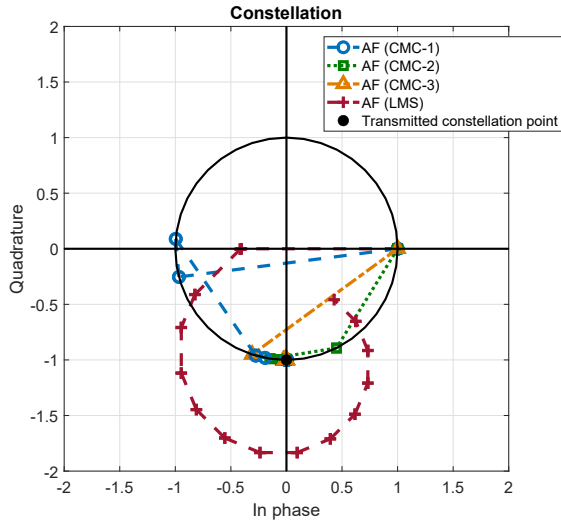

Fig. 9. Dynamics of CMC and LMS mechanisms for a QPSK signal.
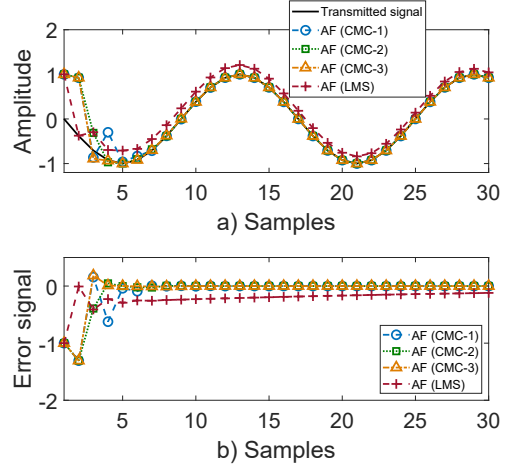

Fig. 8. Dynamics of the proposed AF-based solution considering CMC and LMS mechanisms for a QPSK signal.
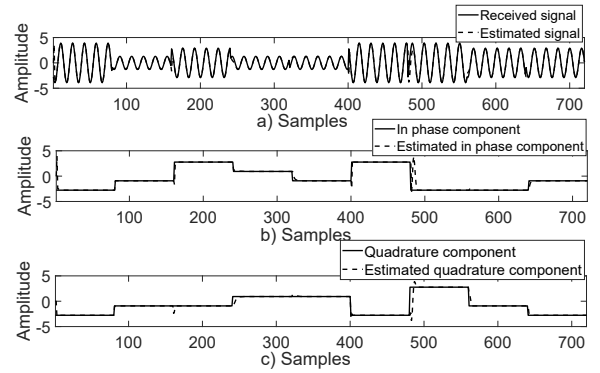

Fig. 10. Illustrative example to recover in-phase and quadrature components of a 16-QAM waveform. a) Transmitted and recovered 16-QAM signal. b) Transmitted and recovered in phase component. c) Transmitted and recovered quadrature component.

output are lower in CMC methods than in LMS. For instance, CMC-1 attains an error signal seven times smaller than the LMS method after 6 iterations achieving a faster convergence rate.

B. QAM Constellation Recovery

To illustrate the extension of the constellation recovery process to QAM signals, we implement the diagram shown in Fig. 5 considering CMC-1 as the updating mechanism of the adaptive filters. A 16-QAM signal is processed with parameters $A_1 = 1.4142$, $A_2 = 3.1623$, and $A_3 = 4.2426$, which correspond to in phase and quadrature amplitudes of ± 1 and ± 3. The remaining modulation parameters were kept as in the QPSK example.

Fig. 10 depicts the estimation of the received signal and its components. As illustrated in this figure, the proposed solution is able to track quite well the in-phase and quadrature

components of the received signal. Just in some transitions, the method exhibits some overshoot effects due to the large difference of amplitude between one symbol and the next.

To further illustrate, Fig. 11 shows the dynamics of the recovery mechanism in the I-Q plane. This figure depicts the transition between two constellation points from the inner circumference to the outer circumference. The initial point is located at $\varphi = -\frac{3\pi}{4}$ in the inner circumference, while the second one is at $\varphi = -\frac{\pi}{4}$ in the outer circumference. As exhibited here, the estimated constellation points first switch from the inner circumference to the outer one, and then start to get closer to the desired point.

VI. SIMULATION RESULTS

To evaluate the merit of the proposed adaptive scheme in a CR scenario, conclusions are drawn from results obtained on simulations and accounting for a variety of channel models. Their analysis accounts for the speed of convergence of the proposed methodology and its capability to diminish the impact of multipath channels, as described in Sections VI-A and VI-B, respectively. Besides, here we consider emissions from a single PU only and noise is modeled as additive white Gaussian noise (AWGN). Multiple interfering sources and the impact of tone capture effect [31], [32] will be addressed as a future outlook.
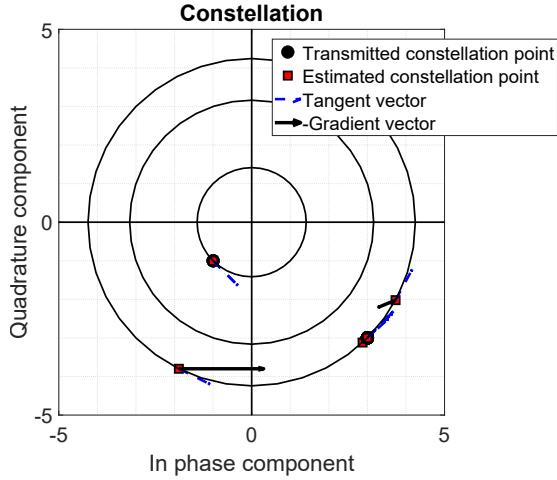
Fig. 11. Dynamics in the I-Q plane of the proposed AF-based solution considering CMC mechanisms for a 16-QAM signal.

Fig. 12. Learning curves for QPSK waveforms when SNR $= \infty$ dB.

Fig. 13. Learning curves for QPSK waveforms when SNR $= 10$ dB.

The input sequences to obtain these metrics consist of BPSK, QPSK, 8PSK, and 16PSK waveforms processed in the discrete-time domain, the normalized carrier frequency is located at $\omega_c = \frac{\pi}{8}$ and the amplitude is $A = 1$. We use the same normalized frequency following CR systems as explained in the previous Section. Data is randomly generated following a uniform distribution and for simulation's purposes, the bit length is 80 samples (according to duration as five times the carrier period). For the LMS algorithm, the adaptive step-size is selected as $\mu = \frac{0.9}{\lambda_{max}}$ to achieve a faster speed of convergence, where λ_{max} is defined in Eq. (12). The same value for λ is selected in the case of the CMC methods.

Simulations are obtained in comparison to the Costas Loop (cf. Fig. 2 a)) combined with CMA method. In this connection, the received signal is pre-processed with the CMA method to compensate for the channel impact following the solution reported by Godard [23]. Besides, the CMA equalizer is implemented by 2 complex tap gains to have a fair comparison with the proposed system in Fig. 3. The adaptive step size is selected as $\frac{1}{200 \cdot 30 \mathbb{E}\{a_n^2\}}$ [23], where $\mathbb{E}\{a_n^2\}$ represents the variance of the transmitted symbols, where $\mathbb{E}\{\cdot\}$ is the statistical mean operator.

A. Speed of Convergence

The speed of convergence is measured by considering the learning curve based on the mean squared error (MSE) criteria as $\mathbb{E}\{e^2[n]\}$, and $e^2[n]$ is the difference between the estimated sequence and the transmitted one. To illustrate the speed of convergence performance, 200 iterations were performed with different initialization of data, noise, and coefficients values for QPSK waveforms.

Figures 12 to 15 depict the MSE criteria for a variety of SNR values, i.e., infinite (not noise), 10, 5 and 0 dB. According to Fig. 12, where the channel is assumed ideal (without noise and multipaht effects), the proposed AF-based scheme (cf. Fig. 3) has better performance in comparison to the Costas Loop method (cf. Fig. 2 a)) combined with CMA. Besides, the CMC methods exhibit a better speed of convergence in comparison to LMS. In this case, the CMC methods
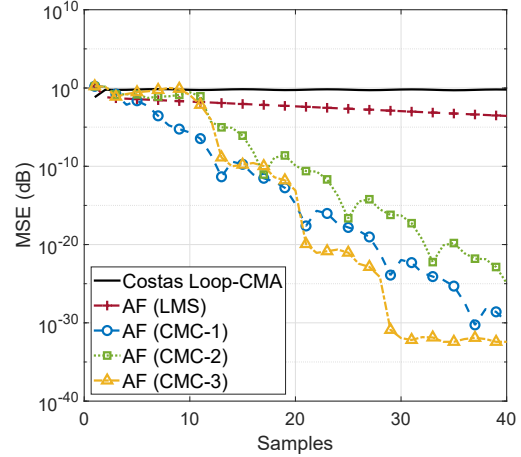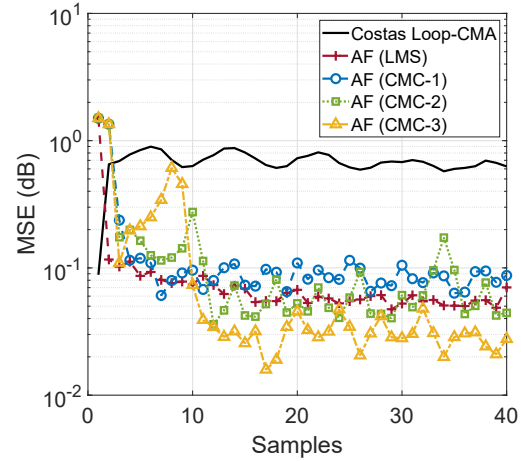
dramatically decline as the number of iterations increases and CMC-3 presents the best behavior. In the presence of AWGN, from Figures 13 to 15, CMC-3 presents the highest speed of convergence.

Additionally, the MSE performance for other modulation orders is also illustrated in Fig. 16 when SNR = 10 dB. This figure exhibits a similar performance for the proposed scheme when using CMC-3 and considering a variety of modulation schemes such as QPSK, 8PSK, and 16PSK waveforms.

B. Inter-symbol Interference

The distortion produced by multipath channels and its limited bandwidth leads to ISI effects on the recovered in-phase and quadrature levels, which in turn deteriorates the quality of communications. To demonstrate the feasibility of the proposed AF-based scheme in Fig. 3, by using the algorithms LMS and CMC-1 to CMC-3, we simulate a variety of real FIR and infinite impulse response (IIR) channels from [33]–[37].

Provided that the channel attenuates the transmitted signal, in the proposed AF-based scheme the amplitude of the received signal is estimated similarly to the CMA method as $\widehat{A} = \frac{\mathbb{E}|r[n]|^4}{\mathbb{E}|r[n]|^2}$, as indicated in Section IV. Under these
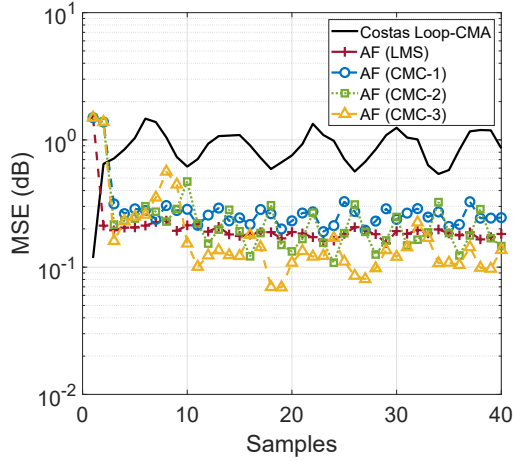
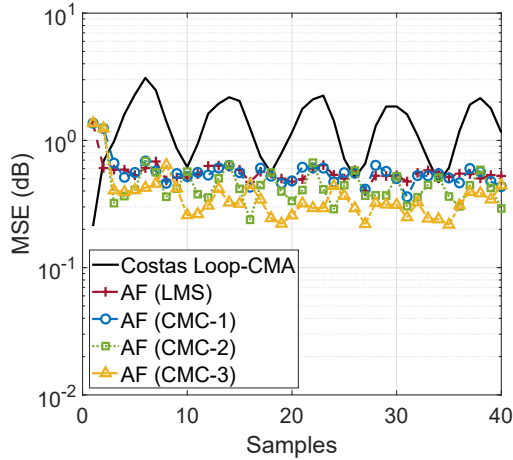Fig. 14. Learning curves for QPSK waveforms when SNR = 5 dB.

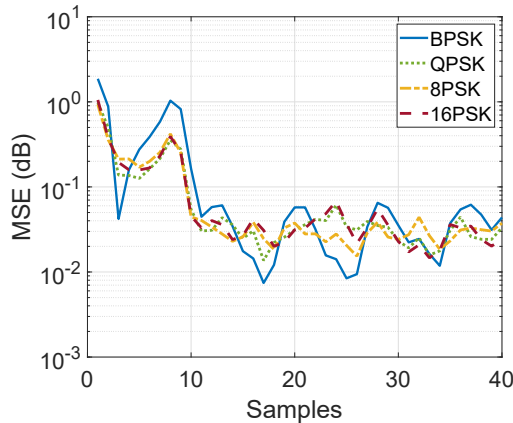Fig. 15. Learning curves for QPSK waveforms when SNR = 0 dB.

Fig. 16. Learning curves for QPSK, 8PSK, and 16PSK waveforms utilizing the AF-based scheme and considering CMC-3 when SNR = 10 dB.
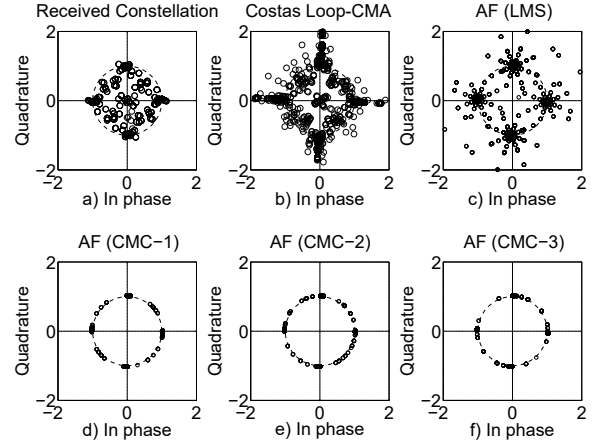

Fig. 17. Recovered constellation points for transmissions over the FIR channel provided by Johnson and Sethares [33]. a) Received constellation points, b) Costas Loop+CMA, c) AF (LMS), d) AF (CMC-1), e) AF (CMC-2), f) AF (CMC-3) methods.
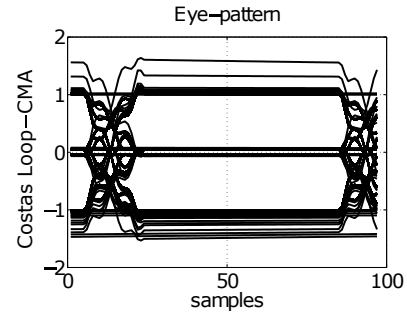

Fig. 18. Eye-pattern of the Costas Loop scheme combined with CMA for transmissions in the FIR channel provided by Johnson and Sethares [33].

assumptions, we demonstrate the effectiveness of the proposed solutions by obtaining constellation and eye pattern diagrams for 8000 iterations.

1) FIR channel: In this example, we consider a tap FIR filter to model multipath channel distortions. The multipath channel is modeled through the impulse response vector $h[n] = [0.5, \ 1, \ -0.6]$ [33]. Fig. 17 illustrates the constellation points regarding the received constellation in a), the Costas Loop scheme combined with CMA in b), as well as the proposed AF-based scheme according to LMS in c), CMC-1 in d), CMC-2 in e), and CMC-3 in f). As observed in Fig. 17 d) to f), the proposed AF-based methods CMC-1 to CMC-3 reduce the spreading of the constellation points in comparison to CMA and LMS algorithms. Figures 18 and 19 show the eye-opening behavior for the Costas Loop and the proposed solutions, respectively. The methods CMC-1 to CMC-3 lead to a clear eye-opening pattern, which in turn favors the proper detection of the received phase.

Additionally, we also simulated the SUI-3 channel model [34], where the impulse response vector is $h_i[n] = [0.5395, 0.0451, -0.1025]$ and $h_q[n] = [-0.0607, \ -0.119, \ -0.1126]$, respectively. Fig. 20 a) to f) illustrate the received and recovered constellation points for each method, while Figures 21 and 22 depict the eye-opening pattern for Costas Loop combined with CMA
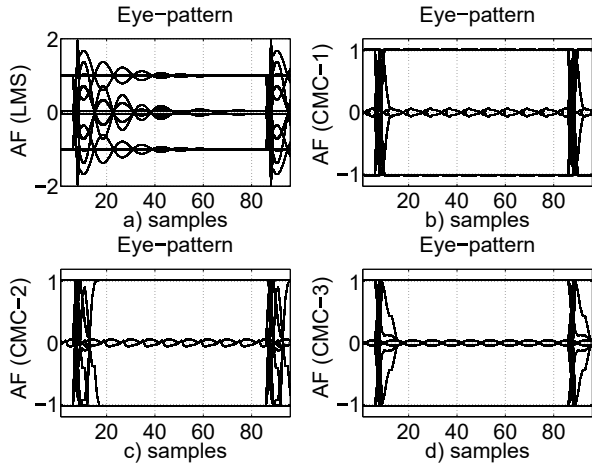
Fig. 19. Eye-patterns for transmissions in the FIR channel provided by Johnson and Sethares [33]. a) AF (LMS), b) AF (CMC-1), c) AF (CMC-2), d) AF (CMC-3) methods.
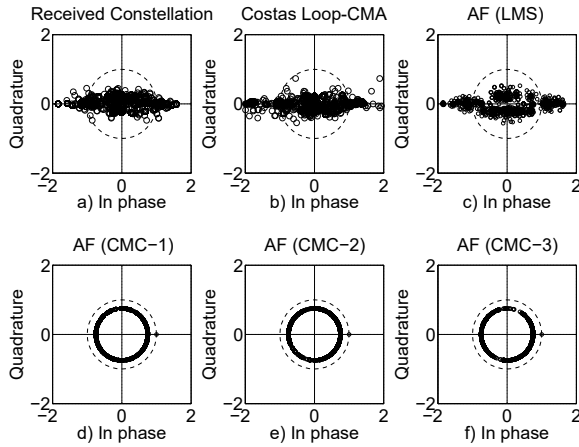

Fig. 20. Recovered constellation points for transmissions in the SUI-3 channel in [34]. a) Received constellation points, b) Costas Loop+CMA, c) AF (LMS), d) AF (CMC-1), e) AF (CMC-2), f) AF (CMC-3) methods.

and the proposed AF-based method, respectively. Fig. 20 exhibits the superior performance of the proposed AF-based scheme in comparison to the Costas Loop with CMA when recovering the constellation points. Similar behavior is obtained regarding the eye-opening pattern when comparing the proposed AF-based method in Fig. 22 a) to the Costas Loop with CMA in Fig. 21.

2) Non-minimum phase channel: This example illustrates performance when the channel is modeled by the impulse response vector

$$h[n] = \begin{cases} 0 & n < 0 \\ -0.4 & n = 0 \\ 0.84 \cdot 0.4^n & n > 0 \\ 0 & n >= 7 \end{cases}, \tag{13}$$

which describes a non-minimum phase channel of length 7 samples [35], [36]. Through this channel, results for the recovered constellation points and eye pattern are illustrated in Figures 23 to 25. In this case, the method CMC-2 exhibits a
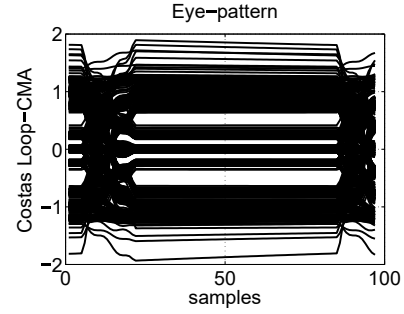

Fig. 21. Eye-pattern derived from the Costas Loop scheme combined with CMA for transmissions in the SUI-3 channel provided in [34].
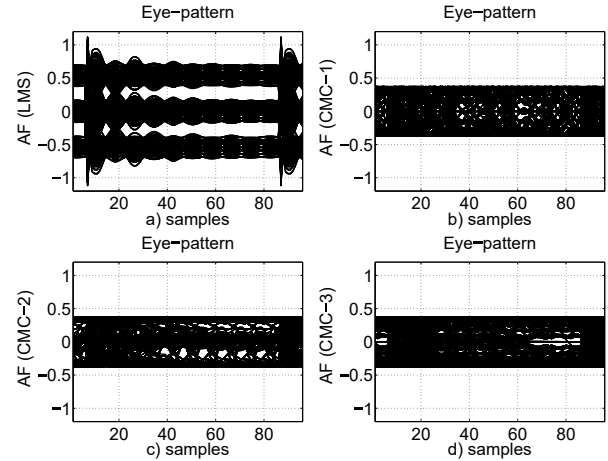

Fig. 22. Eye-patterns for transmissions in the SUI-3 channel provided in [34]. a) AF (LMS), b) AF (CMC-1), c) AF (CMC-2), d) AF (CMC-3) methods.

better eye-opening, and the LMS method a better constellation points recovery when compared to the Costas Loop with CMA scheme.

3) IIR channel: Finally, this section illustrates the performance in the case of IIR channels. The transmitted QPSK signal is then processed by a distortion channel described through its z-transform as [37]

$$H(z) = \frac{1}{1 + 0.9z^{-1}}. \tag{14}$$

Based on this channel, the received and recovered constellation points are shown in Fig. 26, the resulting eye pattern is illustrated in Figures 27 and 28. In this case, the Costas Loop scheme combined with CMA, AF-based CMC-1, and AF-based CMC-2 methods present a similar performance on clustering the constellation points and in the openness of the eye pattern.

C. Remarks

Regarding the mitigation of channel distortion, the obtained results demonstrate to have a good performance when using the proposed AF-based scheme with the CMC methods. The imposed restriction, regarding the constant amplitude, introduces an advantage to reduce distortion in comparison to the traditional Costas Loop combined with CMA. In general, the adaptive schemes for CMC-1 and CMC-2 methods exhibit
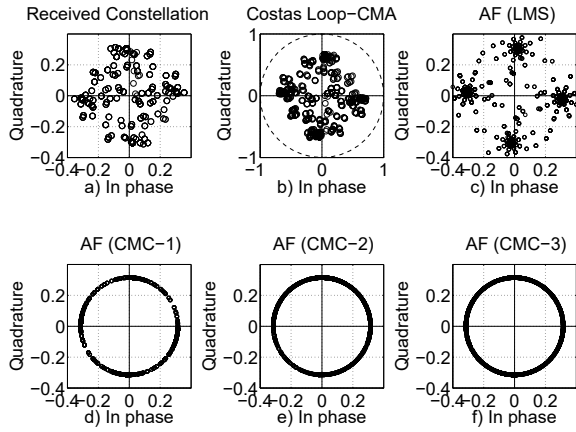
Fig. 23. Recovered constellation points for transmissions in the non-minimum phase channel provided by Shalvi and Weinstein [35] and Maricic *et al.* [36]. a) a) Received constellation points, b) Costas Loop+CMA, c) AF (LMS), d) AF (CMC-1), e) AF (CMC-2), f) AF (CMC-3) methods.
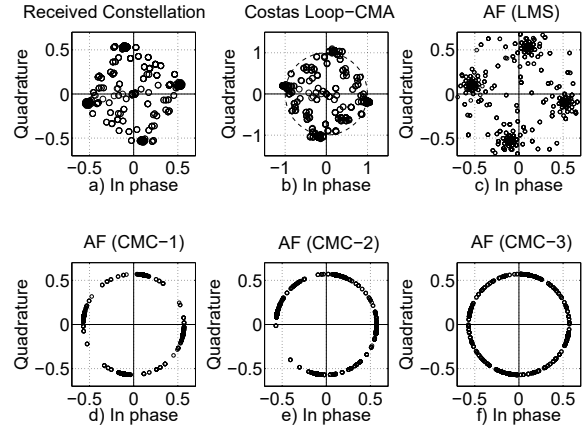

Fig. 26. Recovered constellation points for transmissions over the IIR channel provided by Jones [37]. a) Received constellation points, b) AF (LMS), c) AF (CMC-1), d) AF (CMC-2), e) AF (CMC-3) methods.
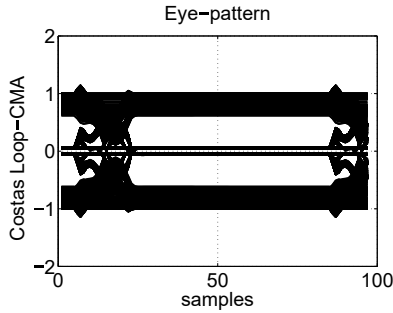

Fig. 24. Eye-pattern of the Costas Loop scheme combined with CMA for transmissions in the non-minimum phase channel provided by Shalvi and Weinstein [35] and Maricic *et al.* [36].

Fig. 27. Eye-pattern of the Costas Loop scheme combined with CMA for transmissions in the IIR channel provided by Jones [37].

Fig. 25. Eye-patterns for transmissions in the non-minimum phase channel provided by Shalvi and Weinstein [35] and Maricic *et al.* [36]. a) AF (LMS), b) AF (CMC-1), c) AF (CMC-2), and d) AF (CMC-3) methods.
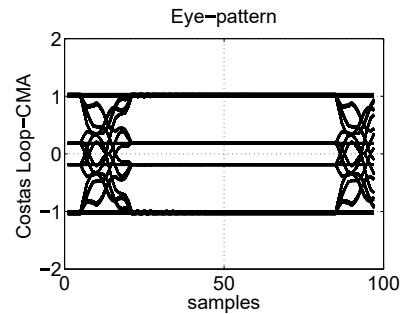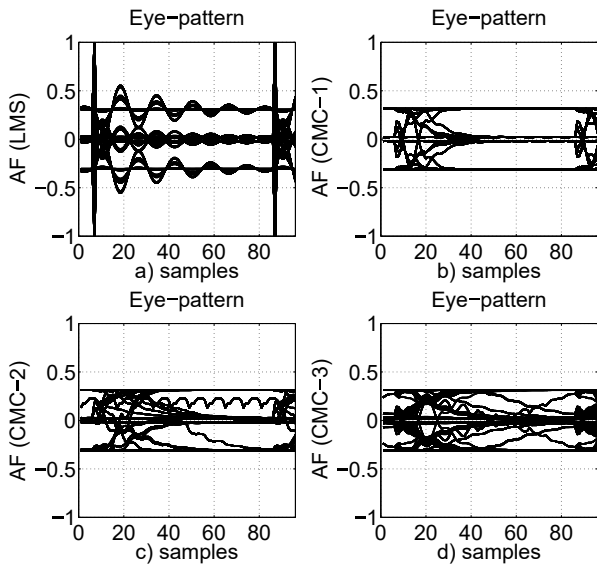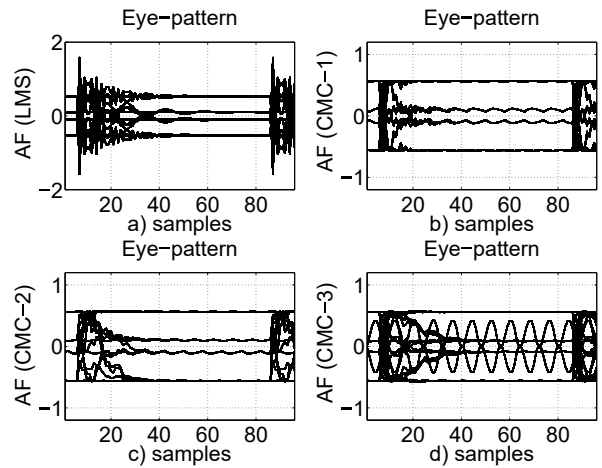

Fig. 28. Eye-patterns for transmissions in the IIR channel provided by Jones [37]. a) AF (LMS), b) AF (CMC-1), c) AF (CMC-2), and d) AF (CMC-3) methods.

better performance to mitigate the impact of multipath channel environments when recovering the constellation points and in the opening of the eye pattern. Future directions will be conducted on the testbeds implementation of the proposed mechanisms. Using SDR boxes the real-time operation of this method may be tested on wireless links.

VII. CONCLUSIONS

A low complex scheme, to jointly equalize and recover the constellation points from PSK waveforms, is conceived when utilizing an adaptive filter scheme. The system operates without a training sequence, which in turn represents a strong capability to operate on AMR applications. Also, it exhibits less complexity than existing blind schemes like the traditional Costas Loop combined with CMA. Taking advantage of the constant amplitude of PSK waveforms, the proposed AF-based scheme can profit from new coefficients update mechanisms, named CMC, that provides robust performance, not only recovering constellation points but also reducing performance degradation produced by ISI. Additionally, simulation results confirm the improved speed of convergence of the proposed AF-based schemes with CMC methods when compared to the Costas Loop scheme combined with CMA. Future directions will be conducted on the testbeds implementation of the proposed mechanisms. Using software defined radio (SDR) boxes the real-time operation of this method may be tested on wireless links. Furthermore, the proposed solution may be extended to consider multiples sources and the impact of interference as well as the tone capture effect.

REFERENCES

[1] T. Aldalgamouni, M. C. Ilter, and H. Yanikomeroglu, "Joint Power Allocation and Constellation Design for Cognitive Radio Systems," *IEEE Transactions on Vehicular Technology (TVT)*, vol. 67, no. 5, pp. 4661–4665, May 2018.

[2] "Cisco Annual Internet Report (2018–2023) White Paper," CISCO, Tech. Rep., Mar. 2020, pp. 1–35. [Online]. Available: https://www.cisco.com/c/en/us/solutions/collateral/executive-perspectives/annual-internet-report/white-paper-c11-741490.pdf (visited on 08/10/2021).

[3] J. Mitola and Maguire, Jr., G. Q., "Cognitive radio: making software radios more personal," *IEEE Personal Communications*, vol. 6, no. 4, pp. 13–18, Aug. 1999.

[4] Y.-C. Liang, K.-C. Chen, G. Y. Li, and P. Mahonen, "Cognitive radio networking and communications: an overview," *IEEE Transactions on Vehicular Technology (TVT)*, vol. 60, no. 7, pp. 3386–3407, Sep. 2011.

[5] O. A. Dobre, "Signal identification for emerging intelligent radios: classical problems and new challenges," *IEEE Instrumentation & Measurement Magazine*, vol. 18, no. 2, pp. 11–18, Apr. 2015.

[6] J. Mitola, A. Attar, H. Zhang, O. Holland, H. Harada, and H. Aghvami, "Achievements and the Road Ahead: The First Decade of Cognitive Radio," *IEEE Transactions on Vehicular Technology (TVT)*, vol. 59, no. 4, pp. 1574–1577, May 2010.

[7] O. A. Dobre, A. Abdi, Y. Bar-Ness, and W. Su, "Survey of automatic modulation classification techniques: classical approaches and new trends," *IET Communications*, vol. 1, no. 2, p. 137, 2007.

[8] Darsena, Donatella and Gelli, G. and Verde, F., "An Opportunistic Spectrum Access Scheme for Multicarrier Cognitive Sensor Networks," *IEEE Sensors Journal*, vol. 17, no. 8, 2596–2606, Apr 2017.

[9] T. Yucek and H. Arslan, "A survey of spectrum sensing algorithms for cognitive radio applications," *IEEE Communications Surveys & Tutorials*, vol. 11, no. 1, pp. 116–130, Mar. 2009.

[10] G. Matz and F. Hlawatsch, "Fundamentals of Time-Varying Communication Channels," in *Wireless Communications Over Rapidly Time-Varying Channels*, F. Hlawatsch and G. Matz, Eds., Elsevier, 2011, pp. 1–63.

[11] Sushma, Venkataratnam, and S. Yellampalli, "A low-area based costas loop implementation for BPSK signals," in *International Conference on Electrical, Electronics, Communication, Computer, and Optimization Techniques (ICEECCOT 2017)*, Mysore, India: IEEE, Dec. 2017.

[12] M. Ayat, S. Mirzakuchaki, and A. Beheshti-Shirazi, "Design and Implementation of High Throughput, Robust, Parallel M-QAM Demodulator in Digital Communication Receivers," *IEEE Transactions on Circuits and Systems I: Regular Papers*, vol. 63, no. 8, pp. 1295–1304, Aug. 2016.

[13] A. O. A. Salam, R. E. Sheriff, Y.-F. Hu, S. R. Al-Araji, and K. Mezher, "Automatic Modulation Classification Using Interacting Multiple Model Kalman Filter for Channel Estimation," *IEEE Transactions on Vehicular Technology (TVT)*, vol. 68, no. 2, pp. 8928–8939, Feb. 2019.

[14] S. Haykin, *Adaptive filter theory*, 5th ed. Lakewood, NJ: Prentice Hall, 2013.

[15] B. Widrow, J. Glover, J. McCool, J. Kaunitz, C. Williams, R. Hearn, J. Zeidler, J. E. Dong, and R. Goodlin, "Adaptive noise cancelling: Principles and applications," *Proceedings of the IEEE*, vol. 63, no. 12, pp. 1692–1716, 1975.

[16] D. Giardino, G. C. Cardarilli, L. D. Nunzio, R. Fazzolari, A. Nannarelli, M. Re, and S. Spano, "M-PSK Demodulator With Joint Carrier and Timing Recovery," *IEEE Transactions on Circuits and Systems II: Express Briefs (TCAS-II)*, vol. 68, no. 6, pp. 1912–1916, Jun. 2021.

[17] T. R. Roshna, R. Nivin, J. Sherly, J. AprenT, and V. Alex, "Design and implementation of digital Costas loop and Bit synchronizer in FPGA for BPSK demodulation," in *International Conference on Control Communication and Computing (ICCC 2013)*, Thiruvananthapuram, India: IEEE, Dec. 2013.

[18] J. L. Xu, W. Su, and M. Zhou, "Software-Defined Radio Equipped With Rapid Modulation Recognition," *IEEE Transactions on Vehicular Technology (TVT)*, vol. 59, no. 4, pp. 1659–1667, May 2010.

[19] H.-D. Han, Z. Ding, and M. Zia, "A Convex Relaxation Approach to Higher-Order Statistical Approaches to Signal Recovery," *IEEE Transactions on Vehicular Technology (TVT)*, vol. 66, no. 1, pp. 1–1, Jan. 2017.

[20] V. Zarzoso and P. Comon, "Optimal Step-Size Constant Modulus Algorithm," *IEEE Transactions on Communications*, vol. 56, no. 1, pp. 10–13, Jan. 2008.

[21] J. Proakis and M. Salehi, *Digital communications*, 5th ed., ser. McGraw-Hill higher education. McGraw-Hill, 2008.

[22] R. Zhu, F. Yang, and J. Yang, "An RLS-Based Lattice-Form Complex Adaptive Notch Filter," *IEEE Signal Processing Letters*, vol. 23, no. 2, pp. 217–221, Feb. 2016.

[23] D. Godard, "Self-Recovering Equalization and Carrier Tracking in Two-Dimensional Data Communication Systems," *IEEE Transactions on Communications*, vol. 28, no. 11, pp. 1867–1875, Nov. 1980.

[24] P. Peebles Z., *Probability, random variables, and random signal principles*. Albany, NY: McGraw-Hill, Inc., 1987, p. 352.

[25] S. Kay, *Fundamentals of Statistical Signal Processing: Estimation Theory*. Upper Saddle River, NJ: Prentice Hall, 1998.

[26] G. Velarde-Torres, "CMA equalization with decision-directed phase correction," in *Conference Record of the Thirty-Eighth Asilomar Conference on Signals, Systems and Computers, 2004*, vol. 2, Pacific Grove, CA: IEEE, Nov. 2004, pp. 2047–2050.

[27] M. Luis, R. Oliveira, R. Dinis, and L. Bernardo, "RF-Spectrum Opportunities for Cognitive Radio Networks Operating Over GSM Channels," *IEEE Transactions on Cognitive Communications and Networking (TCCN)*, vol. 3, no. 4, pp. 731–739, Dec. 2017.

[28] K. Bani and V. Kulkarni, "Simulation and Analysis of IEEE 802.22 Cognitive Radio Network," in *International Conference on Convergence to Digital World - Quo Vadis (ICCDW 2020)*, Mumbai, India: IEEE, Feb. 2020.

[29] *Selection Table for High Speed A/D Converters > 10 MSPS / Parametric Search / Analog Devices*, 2021. [Online]. Available: https://www.analog.com/en/parametricsearch/11814#/p1746=20M%7C20M (visited on 10/17/2021).

[30] A. B. Carlson, P. B. Crilly, and J. C. Rutledge, *Communication Systems: An Introduction to Signals and Noise in Electrical Communication*, 4th ed. New York City, NY: McGraw-Hill, 2002.

[31] Treichler, J. and Larimore, M., "The tone capture properties of CMA-based interference suppressors," *IEEE Transactions on Acoustics, Speech, and Signal Processing*, vol. 33, no. 4, 946–958, Aug 1985.

[32] Gelli, G. and Verde, F., "Two-stage interference-resistant adaptive periodically time-varying CMA blind equalization," *IEEE Transactions on Signal Processing*, vol. 50, no. 3, 662–672, Mar 2002.

[33] C. R. Johnson and W. A. Sethares, *Telecommunications Breakdown: Concepts of Communication Transmitted via Software-Defined Radio*. Upper Saddle River, NJ: Prentice Hall, 2003.

[34] IEEE, "Channel Models for Fixed Wireless Applications," Institute of Electrical and Electronics Engineers (IEEE), Std 802.16a-03, Jun. 2003.

[35] O. Shalvi and E. Weinstein, "New criteria for blind deconvolution of nonminimum phase systems (channels)," *IEEE Transactions on Information Theory*, vol. 36, no. 2, pp. 312–321, Mar. 1990.

[36] B. Maricic, Z.-Q. Luo, and T. Davidson, "Blind constant modulus equalization via convex optimization," *IEEE Transactions on Signal Processing*, vol. 51, no. 3, pp. 805–818, Mar. 2003.

[37] D. Jones, "A normalized constant-modulus algorithm," in *29th Asilomar Conference on Signals, Systems and Computers*, vol. 1, Pacific Grove, CA: IEEE, Nov. 1995, 694–697 vol.1.

Liset Martínez Marrero received her B.Sc. (2013) and M.Sc. (2019) degrees from the Havana University of Technology, CUJAE, Cuba. Currently, she collaborates with the Competence Center - Intelligent Sensors and Networks (CC-ISN) at the Lucerne University of Applied Sciences and Arts (HSLU), Switzerland. Her research interests include digital communications systems, DSP, and Power Line Communications.

Jorge Torres Gómez received the B.Sc. (2008), M.Sc. (2010), and Ph.D. (2015) degrees from the Havana University of Technology, CUJAE, Cuba. He is currently with the School of Electrical Engineering and Computer Science, TU Berlin. From 2008 to 2018, he lectured with the School of Telecommunications and Electronics, CUJAE. He has been with the Department of Signal Theory and Communications, UC3M, Spain, as a guest lecturer, and with the TU Chemnitz as a postdoc. He is with the committee of Teaching and Professional Activities in the IEEE German Chapter, Executive Committee. His research interests include DSP, SDR, and Education. He has been participating in DAAD, Erasmus+ and CAPES research projects. He is reviewer of Physical Communication, RIELAC and Telematic journals, as well as Vehicular Technology Conference (VTC).

Falko Dressler is full professor and Chair for Data Communications and Networking at the School of Electrical Engineering and Computer Science, TU Berlin. He received his M.Sc. and Ph.D. degrees from the Dept. of Computer Science, University of Erlangen in 1998 and 2003, respectively. Dr. Dressler has been associate editor-in-chief for IEEE Trans. on Mobile Computing and Elsevier Computer Communications as well as an editor for journals such as IEEE/ACM Trans. on Networking, IEEE Trans. on Network Science and Engineering, Elsevier Ad Hoc Networks, and Elsevier Nano Communication Networks. He has been chairing conferences such as IEEE INFOCOM, ACM MobiSys, ACM MobiHoc, IEEE VNC, IEEE GLOBECOM. He authored the textbooks Self-Organization in Sensor and Actor Networks published by Wiley & Sons and Vehicular Networking published by Cambridge University Press. He has been an IEEE Distinguished Lecturer as well as an ACM Distinguished Speaker. Dr. Dressler is an IEEE Fellow as well as an ACM Distinguished Member. He is a member of the German National Academy of Science and Engineering (acatech). He has been serving on the IEEE COMSOC Conference Council and the ACM SIGMOBILE Executive Committee. His research objectives include adaptive wireless networking (sub-6GHz, mmWave, visible light, molecular communication) and wireless-based sensing with applications in ad hoc and sensor networks, the Internet of Things, and Cyber-Physical Systems.

M. Julia Fernández-Getino García (S'99 - AM'02 - M'03) received the M. Eng. and Ph.D. degrees in telecommunication engineering from the Polytechnic University of Madrid, Spain, in 1996 and 2001, respectively. She is currently with the Department of Signal Theory and Communications, Carlos III University of Madrid, Spain, as an Associate Professor. From 1996 to 2001, she held a research position with the Department of Signals, Systems and Radiocommunications, Polytechnic University of Madrid. She visited Bell Laboratories, Murray Hill, NJ, USA, in 1998; visited Lund University, Sweden, during two periods in 1999 and 2000; visited Politecnico di Torino, Italy, in 2003 and 2004; and visited Aveiro University, Portugal, in 2009 and 2010. Her research interests include multicarrier communications, coding and signal processing for wireless systems.

She received the best "Master Thesis" and "Ph.D. Thesis" awards from the Professional Association of Telecommunication Engineers of Spain in 1998 and 2003, respectively; the "Student Paper Award" at the IEEE International Symposium on Personal, Indoor and Mobile Radio Communications (PIMRC) in 1999; the "Certificate of Appreciation" at the IEEE Vehicular Technology Conference (VTC) in 2000; the "Ph.D. Extraordinary Award" from the Polytechnic University of Madrid in 2004; the "Juan de la Cierva National Award" from AENA Foundation in 2004; and the "Excellence Award" from Carlos III University of Madrid in 2012 for her research career.